ARTICLE

Theoretical Study on Resonance Raman Spectra of Tetraoxaporphyrin Dication by TDDFT Calculation

Guo-bing Wang[a], Hui-qing Zhao[b], Zhen-lin Zhang[a], Wen-lou Wang[a], Dong-ming Chen[a*]

a. Department of Chemical Physics, University of Science and Technology of China, Hefei 230026, China

b. Department of Chemistry, College of Basic Medicine, Anhui Medical University, Hefei 230032, China

(Dated: Received on April 13, 2015; Accepted on May 16, 2015)

The B state excited resonance Raman scattering of tetraoxaporphyrin dication (TOP^{2+}) was theoretically studied with DFT/TDDFT calculations and the sum-over-states approach of polarizability including both the A and B terms contributions. The resonance Raman spectra calculated with PBE1PBE, B3LYP, Cam-B3LYP, and B3LYP-D3 functionals are similar to each other in general, with PBE1PBE and B3LYP being better in reproducing resonance Raman intensities in comparison with the experiment. The calculated relative intensities of the totally symmetric modes are excellently consistent with the experiment. The TDDFT calculations manifested a considerable deformation of the B state along the ν_2, ν_6, ν_7, and ν_8 modes, which is responsible for the strong resonance Raman intensities of these modes. The resonance Raman intensities of non-totally symmetric modes were calculated to be weaker than the totally symmetric modes by one or two order of magnitude, which qualitatively agrees with the experiment. However, the resonance Raman intensity of the ν_{10} mode ($C_\beta C_\beta$ stretch, B_{1g} symmetry) predicted by TDDFT calculations is unexpectedly small whereas that of the ν_{11} mode (symmetric $C_\alpha C_m$ stretch, B_{1g} symmetry) is too large, which is assumed to be caused by the Jahn-Teller instability for the B state of TOP^{2+}.

Key words: Tetraoxaporphyrin, Resonance Raman, TDDFT, Excited state structure, Franck-Condon mechanism

I. INTRODUCTION

Tetraoxaporphyrins (TOPs) are a class of porphyrin analogue in which the four pyrrole rings of a normal porphyrin are replaced by four furan rings. These unique compounds received much research interest in the past twenty years since they construct a bridge connecting the porphyrin chemistry and annulene chemistry, and consequently, the studies of TOPs have considerably broadened the knowledge of the corresponding π-electron conjugate systems [1−11]. The discovery of TOPs also opens the door to synthesize other porphyrin-like tetrafuran macrocycles [2−4]. For these reasons, various spectroscopic experiments have been conducted to study the ground and excited state properties of TOPs [1−6, 11]. The dicationic TOP^{2+} is the isoelectronic analogue of normal closed-shell metalloporphyrins (MPs), and it shares many similarities in UV-visible absorption spectra with MPs [1, 6, 11]. On the other hand, Marecelli *et al.* have studied the fluorescence spectrum of TOP^{2+}, and much more intense $S_2 \rightarrow S_0$ fluorescence has been observed for TOP^{2+} as compared with the free-base porphyrin (H_2P) and its diprotonated derivative (H_4P^{2+}) [6]. Bachmann *et al.* have synthesized the TOP radical cation and anion by chemical redox method and the UV-visible-near-IR absorption, emission spectra, and electron spin resonance (ESR) spectra of the redox species were measured and studied [7]. Theoretically, Malsch *et al.* have studied ground state structure of TOP^{2+} using HF, MP2, and density functional theory (DFT) calculations [8]. The importance of electron correlation was demonstrated in order to predict correct ground state structure of TOP^{2+}. Wan *et al.* calculated the electronic excitation energies of TOP^{2+} with TDDFT and found that the observed UV-visible absorption can be well reproduced by taking the solvent effect into account [9]. Xiang *et al.* have theoretically studied the ground-state geometries, ESR isotropic hyperfine coupling constants, and linear vibronic coupling constants of tetraoxaporphyrin monocation/monoanion radicals ($[TOP\cdot]^-$ and $[TOP\cdot]^+$) with DFT calculations [10]. These theoretical and spectroscopic studies have revealed the similarities and contraries between the TOPs and normal porphyrin compounds [6−11].

DFT calculations have been extensively used to study the structures as well as the electronic and vibrational spectra of porphyrin-related compounds. Previously,

*Author to whom correspondence should be addressed. E-mail: dmchen@ustc.edu.cn

Jelovica *et al.* have studied IR absorption and off-resonance Raman (RR) spectra of TOP^{2+} and proposed the assignments of the observed vibrational bands with the assistance of DFT calculations [5]. On the other hand, the resonance Raman scattering (RRS) of TOP^{2+} has been measured [11] but not been theoretically studied yet. It is well known that RRS, as an effective tool for structure characterization and elucidation, plays an important role in porphyrin study [12−19]. Particularly, the properties of the excited state in resonance can be obtained by RR intensity analyses. The RR intensities have been well formulated either in sum-over-states approach or equivalently in the time-dependent picture [20−28]. The Kramers-Kronig transform can also be used to calculate RR intensities from the UV-visible absorption spectrum of the sample.

In this work, we use TDDFT calculations and the sum-over-states formulas of Raman polarizability to study the resonance Raman spectra of TOP^{2+} with B state (S_2 state) excitation, where both the Raman A term (Franck-Condon term) and the B term (Hertzberg-Teller term) were considered. It was demonstrated that the interplay of RR experiments and TDDFT calculations can provide a reliable route to reveal the structures and dynamics of the excited electronic states in resonance.

II. THEORY AND COMPUTATION DETAILS

The differential cross section of Raman scattering ($\pi/4$ scattering geometry) is given by [22, 24, 27]:

$$\frac{\mathrm{d}\sigma}{\mathrm{d}\Omega} = \frac{16\pi^4\nu_L(\nu_L-\nu_k)^3}{30[1-\exp(-hc\nu_k/k_\mathrm{B}T)]}(10\Sigma^0+5\Sigma^1+7\Sigma^2) \quad (1)$$

where ν_k is the vibrational frequency, ν_L is the incident light frequency, c the speed of light, k_B the Boltzmann constant, and h the Planck constant. Σ^0, Σ^1, and Σ^2 in Eq.(1) are the rotational invariants (isotropic, antisymmetric, and anisotropic, respectively) of the Raman tensor [21, 22].

The total cross section of a Raman band is given by [26]:

$$\sigma_\mathrm{R} = \frac{8\pi}{3}\frac{1+2\rho}{1+\rho}\frac{\mathrm{d}\sigma}{\mathrm{d}\Omega} \quad (2)$$

where ρ is the Raman depolarization ratio. The Raman polarizability tensor is given by [20]:

$$\alpha_{\rho\sigma} = \frac{1}{hc}\sum_{M,m}\left(\frac{\langle Gg|\hat{\mu}_\rho|Mm\rangle\langle Mm|\hat{\mu}_\sigma|Gg'\rangle}{\nu_{Mm,Gg}-\nu_\mathrm{L}-i\Gamma} + \frac{\langle Gg|\hat{\mu}_\sigma|Mm\rangle\langle Mm|\hat{\mu}_\rho|Gg'\rangle}{\nu_{Mm,Gg'}+\nu_L+i\Gamma}\right) \quad (3)$$

where the summation covers all the intermediate vibronic states $|Mm\rangle$. In Eq.(3), $|Gg\rangle$ and $|Gg'\rangle$ are the vibronic wavefunctions of the gth and g'th vibrational levels at the electronic ground state G, $|Mm\rangle$ is the vibronic wavefunctions of the mth vibrational level at the electronic excited state M, $\hat{\mu}_\rho$ and $\hat{\mu}_\sigma$ are the electric dipole moment operators. $\nu_{Mm,Gg}$ and $\nu_{Mm,Gg'}$ are the frequency differences between the vibronic states.

Using adiabatic approximation, the electronic and the vibrational wavefunctions can be separated. With Herzberg-Teller expansion, the transition dipole moments can be written as [20]:

$$\langle G|\hat{\mu}_\sigma|M\rangle = \langle G|\hat{\mu}_\sigma|M\rangle_0 + \sum_k\left(\frac{\partial\langle G\,|\hat{\mu}_\sigma|\,M\rangle}{\partial Q_k}\right)_0 Q_k \quad (4)$$

where Q_k is the kth normal coordinate. Accordingly, the Raman polarizability can be expressed into the A term and the B term:

$$\alpha_{\rho\sigma} = A_{\rho\sigma} + B_{\rho\sigma} \quad (5)$$

When only one excited electronic state is involved in resonance Raman, the non-resonance terms can be neglected. By using the harmonic approximation, the two terms can be expressed as [21−24]:

$$A_{\rho\sigma} = \frac{1}{hc}\sum_M\frac{\Delta}{\sqrt{2}}\exp\left(-\frac{\Delta^2}{2}\right)\langle G|\hat{\mu}_\rho|M\rangle_0\langle M|\hat{\mu}_\sigma|G\rangle_0\cdot\left(\frac{1}{\nu_0-\nu_L-i\Gamma}-\frac{1}{\nu_0-\nu_L+\nu_k-i\Gamma}\right) \quad (6)$$

$$B_{\rho\sigma} = \frac{1}{\sqrt{2}hc}\sqrt{\frac{h}{2\pi c\nu_k}}\Bigg\{\sum_M\frac{1}{\nu_0-\nu_L-i\Gamma}\exp\left(-\frac{\Delta^2}{2}\right)\cdot\Bigg[\left(1+\frac{\Delta^2}{2}\right)\langle G|\hat{\mu}_\sigma|M\rangle_0\left(\frac{\partial\langle M|\hat{\mu}_\rho|G\rangle}{\partial Q_k}\right)_0 + \frac{\Delta^2}{2}\langle G|\hat{\mu}_\rho|M\rangle_0\left(\frac{\partial\langle G|\hat{\mu}_\sigma|M\rangle}{\partial Q_k}\right)_0\Bigg] + \sum_M\frac{1}{\nu_0-\nu_L+\nu_k-i\Gamma}\exp\left(-\frac{\Delta^2}{2}\right)\cdot\Bigg[\langle G|\hat{\mu}_\sigma|M\rangle_0\left(\frac{\partial\langle M|\hat{\mu}_\rho|G\rangle}{\partial Q_k}\right)_0 - \frac{\Delta^2}{2}\langle G|\hat{\mu}_\rho|M\rangle_0\left(\frac{\partial\langle G|\hat{\mu}_\sigma|M\rangle}{\partial Q_k}\right)_0\Bigg]\Bigg\} \quad (7)$$

In Eq.(6) and Eq.(7), ν_0 is the frequency of 0-0 vibronic transition, Δ is the dimensionless displacement of the excited state with respect to the ground state along the kth normal coordinate. Under harmonic approximation, the displacement of the excited state with respect to the ground state can be calculated from the gradient of the excited state PES (potential energy surface) at the ground state geometry [25, 28]. Γ is the line width of the excited electronic state. Eq.(6) shows that the A term sensitively depends on Δ and the transition dipole moment of the excited state in resonance. Eq.(7) shows that the B terms depends on the dimensionless

DOI:10.1063/1674-0068/28/cjcp1504067

displacement Δ, the transition dipole moments, as well as the change of the transition dipole moments induced by molecular vibrations. The Eqs.(1), (2), (6), and (7) were used to calculate RR intensities with the Matlab 7.0 software package.

The ground state geometry of TOP^{2+} was firstly optimized with DFT. Analytical frequency calculation was subsequently carried out to provide harmonic frequencies and the compositions of the normal modes. To calculate the B band excited resonance Raman of TOP^{2+} with Eq.(6) and Eq.(7), we carried out TDDFT calculations at the equilibrium structure and also at the structures deformed along each specific modes. The results of TDDFT were used to numerically calculate the gradient of the excited state PES (for calculating the displacement Δ) and the partial derivatives of transition dipole with respect to the normal modes. Two-point differential method was utilized in numerical derivative calculations. A small step size of normal coordinates (0.01 Å/Dalton$^{1/2}$) was used to ensure obtaining converged results.

DFT and TDDFT calculations were performed with the Gaussian 09 program suite [29]. We have used four exchange-correlation (XC) functionals in this study, including the Becke's three-parameter hybrid density functional (referred as B3LYP) [30, 31], the one-parameter modified Perdew-Burke-Ernzerhof's functional (PBE1PBE) [32], Handy *et al.*'s long range corrected version of B3LYP using the Coulomb-attenuating method (Cam-B3LYP) [33], as well as the Grimme's dispersion corrected version of B3LYP (B3LYP-D3) [34]. These specific XC-functionals were chosen because they are widely used and have been proven to produce good results for the ground state structures/vibrations as well as for the excited state properties with TDDFT calculations. The standard 6-31G(d) basis sets were used for all DFT/TDDFT calculations.

III. RESULTS

A. Ground state structure and electronic absorption spectrum

The ground state TOP^{2+} dication was calculated to be a planer D_{4h} structure, which is consistent with the spectroscopic experiments and previous theoretical calculations [6, 8−10]. The calculated structural parameters using four XC-functionals are well consistent with each other, with the derivations of the bond-distances and bond-angles less than 0.01 Å and 0.3°, respectively. Figure 1 shows the sketch of TOP^{2+} together with the atomic labels and the selected structural parameters by PBE1PBE/6-31G(d) calculation.

The TOP^{2+} dication has the same number of π-electron as the normal porphyrin macrocycles, and it is not surprising that TOP^{2+} can give rise to similar electronic absorption to normal metalloporphyins, such as zinc porphyrin (ZnP). Experimentally, a strong absorption at 367 nm (B band) and a weak band at 524 nm (Q band) were observed in the UV-visible spectrum of TOP^{2+} [6, 11]. The oscillator strengths of B and Q bands have been measured to be approximately 2.0 and 0.046, respectively [6].

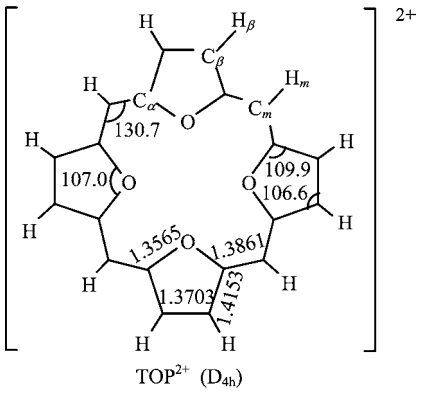

FIG. 1 Schematic diagrams showing the structure of TOP^{2+} with the atomic labels and the key structural parameters calculated by PBE1PBE/6-31G(d). Bond length is in Å, bond angle is in (°).

Table I lists the excitation energies, transition dipole moments, and oscillator strengths of TOP^{2+} calculated with TDDFT. As shown in Table I, the four exchange-correlation functionals give rise to consistent results in general, despite the fact that small differences exist in the computed excitation energies and oscillator strengths by different XC-functionals. According to the TD-PBE1PBE calculation, the first excited state (S_1) of TOP^{2+} is the 1^1E_u state (2.4126 eV, f=0.001) that can be assigned to the weak Q band in the absorption spectrum. This state is described as the combination of the one-electron excitations from the HOMO ($3a_{2u}$) and HOMO-1 ($1a_{1u}$), respectively, to the degenerate LUMO ($4e_g$), and the components of the excited configurations are 49.7% for both $1a_{1u}\rightarrow 4e_g$ and $3a_{1u}\rightarrow 4e_g$ excitations. The second excited state (S_2), 2^1E_u, has large oscillator strength (3.8521 eV, f=3.201 by TD-PBE1PBE), and it can be assigned without doubt to the strong B band in the absorption spectrum. The 2^1E_u state is also originated from the transition from the HOMO/HOMO-1 to the degenerate LUMO, with the principal configurations $1a_{1u}\rightarrow 4e_g$ (46.2%) and $3a_{2u}\rightarrow 4e_g$ excitations (46.2%). These results indicate that the traditional four-orbital model for UV-visible spectra of porphyrin compounds describes very well for the Q and B states of TOP^{2+}. Compared with the experiment, all the four XC-functionals moderately overestimate the oscillator strength of the B band while considerably underestimate that of the Q band. We have noticed that the TDDFT calculations usually give rise to smaller oscillator strength for the Q band of porphyrin compounds as compared with experiments [35].

DOI:10.1063/1674-0068/28/cjcp1504067

TABLE I TDDFT calculated excited state energies (ΔE), transition dipole moments μ, and oscillate strengths f for the electric dipole allowed transitions of TOP^{2+}.

		ΔE/eV	μ_x/a.u.	μ_y/a.u.	f	Assignment
TD-PBE1PBE1	1^1E_u	2.4126	0.0000	0.0876	0.0005	Q_y
		2.4126	0.0876	0.0000	0.0005	Q_x
	2^1E_u	3.8521	0.0000	−4.1182	1.6006	B_y
		3.8521	4.1182	0.0000	1.6006	B_x
	3^1E_u	4.5103	0.0000	−0.4751	0.0249	N_y
		4.5103	−0.4751	0.0000	0.0249	N_x
TD-B3LYP	1^1E_u	2.3577	0.0000	0.1064	0.0007	Q_y
		2.3577	0.1064	0.0000	0.0007	Q_x
	2^1E_u	3.7808	0.0000	−4.0968	1.5547	B_y
		3.7808	4.0968	0.0000	1.5547	B_x
	3^1E_u	4.3058	0.0000	−0.5435	0.0312	N_y
		4.3058	−0.5435	0.0000	0.0312	N_x
TD-Cam-B3LYP	1^1E_u	2.2891	0.0000	−0.0293	<0.0001	Q_y
		2.2891	0.0293	0.0000	<0.0001	Q_x
	2^1E_u	3.9093	0.0000	4.1602	1.6576	B_y
		3.9093	4.1602	0.0000	1.6576	B_x
	3^1E_u	5.0049	0.0000	0.3219	0.0127	N_y
		5.0049	−0.3219	0.0000	0.0127	N_x
TD-B3LYP-D3	1^1E_u	2.3603	0.0000	0.1001	0.0006	Q_y
		2.3603	0.1001	0.0000	0.0006	Q_x
	2^1E_u	3.7837	0.0000	−4.0929	1.5528	B_y
		3.7837	4.0929	0.0000	1.5528	B_x
	3^1E_u	4.3109	0.0000	−0.5490	0.0318	N_y
		4.3109	−0.5490	0.0000	0.0318	N_x

Note: basis sets: 6-31G(d). μ_z=0 for all listed states.

B. Resonance Raman spectra of TOP^{2+} with B band excitation

The molecular vibrations of TOP^{2+} can be divided into the in-plane (ip) and the out-of-plane (oop) modes. It has 36 atoms and $3n-6$=102 degree of internal freedom, which, according to the D_{4h} group, can be classified as

Γ_{ip}=9A_{1g}+9B_{1g}+8A_{2g}+9B_{2g}+17E_u

Γ_{oop}=4A_{1u}+5B_{1u}+5A_{2u}+4B_{2u}+9E_g

Table II shows a classification of the normal modes according to the symmetry species, in which the mode numbers and local coordinates are adapted from the normal D_{4h} metalloporphyrins [12−14]. Among these vibrations, the A_{2u} and E_u modes are IR active, and the A_{1g}, B_{1g}, B_{2g}, and E_g modes are active for off-resonance Raman [12−15]. Resonance Raman is very different from non-resonance Raman in the physical mechanism and in the selection rules. For non-resonance Raman in which the incident light is far from any electronic transitions, the A term contribution to Raman polarizability is much smaller compared with the B term, and A term can be neglected for most cases. For resonance Raman in which the incident irradiation is resonant with an electronic transition, Raman signals can be enhanced either due to the non-zero Frank-Condon overlap between the ground and the resonant excited state (A term mechanism) or due to the vibronic coupling between electronic states (B-term mechanism). It is well known that the A-term mechanism is dominant when the incident radiation is in resonance with a strong electronic transition. For a resonance Raman process involving a single π-π^* electronic transition, only the in-plane modes are expected to be enhanced [12−15]. Also, the A_{2g} and E_u modes are forbidden by symmetry, although the A_{2g} modes may be activated by interstate vibronic coupling between the B and Q electronic states. Thus in the present study we only deal with the A_{1g}, B_{1g}, and B_{2g} modes of TOP^{2+}.

Table III lists the measured and DFT-calculated frequencies for the A_{1g}, B_{1g}, and B_{2g} modes of TOP^{2+}, where the calculated frequencies are scaled with appropriate factors to account for the systematic deviation of the calculations caused by neglect of anharmonicity, the incomplete basis sets, and the use of approximate XC-functionals. The measured relative intensities of RR bands are also listed in Table III. The assignments of

DOI:10.1063/1674-0068/28/cjcp1504067

TABLE II Local coordinate contributions to the in-plane normal modes of TOP^{2+}.

A_{1g}	B_{1g}	A_{2g}	B_{2g}	E_u	Local coordinate[a]	A_{1g}	B_{1g}	A_{2g}	B_{2g}	E_u	Local coordinate[a]
ν_1			ν_{27}	ν_{36}	$\nu(C_mH_m)$			ν_{23}	ν_{31}	ν_{45}	$\nu(C_\beta H_\beta)_{as}$
	ν_{10}	ν_{19}		ν_{37}	$\nu(C_\alpha C_m)_{as}$			ν_{24}	ν_{32}	ν_{46}	δ(Fur def)$_{as}$
ν_2	ν_{11}			ν_{38}	$\nu(C_\beta C_\beta)$	ν_6	ν_{15}			ν_{47}	ν(Fur br)
ν_3			ν_{28}	ν_{39}	$\nu(C_\alpha C_m)_s$	ν_7	ν_{16}			ν_{48}	δ(Fur def)$_s$
		ν_{20}	ν_{29}	ν_{40}	ν(Fur/4)			ν_{26}	ν_{34}	ν_{49}	$\delta(C_\beta H_\beta)_{as}$
ν_4	ν_{12}			ν_{41}	ν(Fur/2)$_s$	ν_9	ν_{17}			ν_{50}	$\delta(C_\beta H_\beta)_s$
	ν_{13}	ν_{21}		ν_{42}	$\delta(C_mH_m)$			ν_{25}	ν_{33}	ν_{51}	δ(Fur rot)
ν_5	ν_{14}			ν_{43}	$\nu(C_\beta H_\beta)_s$	ν_8	ν_{18}		ν_{35}	ν_{52}	δ(Fur transl)
		ν_{22}	ν_{30}	ν_{44}	ν(Fur/2)$_{as}$						

[a] Mode numbering and descriptions are adapted from Ref.[12, 15].

TABLE III Calculated and experimentally measured frequencies for the A_{1g}, B_{1g}, and, B_{2g} modes of TOP^{2+} .

Mode	Frequency/cm^{-1}						Assignment
	PBE1PBE[a]	B3LYP[a]	Cam-B3LYP[a]	B3LYP-D3[a]	Expt.[b]		
A_{1g}	3175	3205	3163	3194		ν_5	$\nu(C_\beta H_\beta)_s$
	3111	3139	3103	3128		ν_1	$\nu(C_mH_m)$
	1539	1539	1543	1539	1536 (0.74)	ν_2	$\nu(C_\beta C_\beta)$
	1423	1426	1430	1425	1421 (0.01)	ν_3	$\nu(C_\alpha C_m)_s$
	1373	1361	1366	1357	1362 (0.19)	ν_4	ν(Fur/2)$_s$
	1060	1077	1064	1074	1069 (0.13)	ν_9	$\delta(C_\beta H_\beta)_s$
	928	928	927	925	934 (1.00)	ν_6	ν(Fur br)
	693	694	693	693	707 (0.41)	ν_7	δ(Fur def)$_s$
	292	294	292	296	304 (0.75)	ν_8	δ(Fur transl)
B_{1g}	3175	3205	3163	3193		ν_{14}	$\nu(C_\beta H_\beta)_s$
	1649	1648	1650	1650	1653 (0.12)	ν_{10}	$\nu(C_\alpha C_m)_{as}$
	1480	1483	1486	1479	1463 (0.03)	ν_{11}	$\nu(C_\beta C_\beta)$
	1378	1382	1376	1384	1369 (0.10)	ν_{12}	ν(Fur/2)$_s$
	1197	1199	1194	1198	1197 (0.05)	ν_{13}	$\delta(C_mH_m)$
	1059	1076	1062	1072	1124 (0.02)	ν_{17}	$\delta(C_\beta H_\beta)_s$
	965	961	962	959		ν_{15}	ν(Fur br)
	720	725	722	728	725 (0.05)	ν_{16}	δ(Fur def)$_s$
	135	137	135	137		ν_{18}	δ(Fur transl)
B_{2g}	3162	3193	3151	3181		ν_{31}	$\nu(C_\beta H_\beta)_{as}$
	3111	3139	3103	3128		ν_{27}	$\nu(C_mH_m)$
	1493	1496	1499	1494		ν_{28}	$\nu(C_\alpha H_m)_s$
	1310	1302	1317	1300	1305 (0.02)	ν_{29}	ν(Fur/4)
	1187	1198	1192	1195		ν_{34}	$\delta(C_\beta H_\beta)_{as}$
	990	984	991	981		ν_{30}	ν(Fur/2)$_{as}$
	792	805	799	803	835 (0.03)	ν_{32}	δ(Fur def)$_{as}$
	416	420	417	421	425 (0.02)	ν_{33}	δ(Fur rot)
	101	104	101	105		ν_{35}	δ(Fur transl)

[a] Basis sets: 6-31G(d). Frequency scaling factor: 0.959, 0.975, 0.956, and 0.972 for PBE1PBE, B3LYP, Cam-B3LYP, and B3LYP-D3, respectively.
[b] The 406.7 nm excited RR spectrum from Ref.[11], relative intensities in parentheses.

DOI:10.1063/1674-0068/28/cjcp1504067

TABLE IV Calculated dimensionless displacements $|\Delta|$ for the B state of TOP^{2+} along the A_{1g} modes.

	Expt. frequency/cm^{-1} [11]	Calculated dimensionless displacement $|\Delta|$[a]			
		PBE1PBE	B3LYP	Cam-B3LYP	B3LYP-D3
ν_2	1536	0.1425	0.1389	0.1555	0.1390
ν_3	1421	0.0370	0.0499	0.0082	0.0472
ν_4	1362	0.0932	0.0823	0.1204	0.0840
ν_9	1069	0.0769	0.0814	0.0788	0.1057
ν_6	934	0.2635	0.2544	0.2602	0.2658
ν_7	707	0.1850	0.2086	0.1943	0.2236
ν_8	304	0.4367	0.5054	0.4307	0.4524

[a] Basis sets: 6-31G(d).

modes were proposed according to the calculated atomic Cartesian displacements for each normal mode.

TDDFT calculations were carried out at the equilibrium structure and also at the structures deformed along each A_{1g}, B_{1g}, and B_{2g} modes. The results of TDDFT were used to numerically calculate the gradient of the excited state PES and the partial derivatives of transition dipole with respect to the normal modes. We are only interested in the normal modes with the frequencies lower than 1700 cm^{-1}, which correspond to the motions of the skeletal C/O atoms of TOP and are expected to be sensitive to the π-π^* electronic excitation. The line width Γ of the B band is taken to be 360 cm^{-1} based on the experimental absorption spectrum [6, 11]. In Ref.[11], the resonance Raman spectrum was recorded by using the 406.7 nm line of a krypton laser as the excitation source, which is red-shifted by 2660 cm^{-1} from the B band absorption (367 nm). This energy difference must be considered in calculation model since it is known that the resonance Raman intensities sensitively depend on the wavelength difference between the incident laser line and the electronic absorption maximum. In addition, the B state energies calculated with TDDFT not only show deviations from the experimental absorption maximum but also vary with different XC-functionals (see Table I). To accord with the experimental conditions, in our Raman intensity calculations the wavelengths of excite light were so chosen that they are red-shifted by 2660 cm^{-1} (0.33 eV) from the corresponding TDDFT-calculated energies of the B state (the 2^1E_u state).

Table IV lists the TDDFT calculated Δ value of B state with respect to the ground state along the totally symmetric A_{1g} modes. The Δ values of non-totally symmetric modes were calculated to be zero. It can be seen from Table IV that the four XC-functionals give rise to comparable Δ values for the corresponding modes. The ν_8, ν_6, ν_7, and ν_2 modes have large Δ values, indicating relatively large deformations of the B state along these modes. Especially, the ν_8 mode has a very large Δ value according to TDDFT calculations (Table IV). This mode, while assigned to furan translation in local coordinate picture, is in fact the expansion vibration of the whole TOP ring. Thus the unusual large Δ value of ν_8 seems reflecting the fact that the π-system of TOP^{2+} contains more anti-bonding character in the B state.

Table V lists the x and y components of the partial derivatives of transition dipole moments $\left(\frac{\partial\langle G|\hat{\mu}_\sigma|M\rangle}{\partial Q_k}\right)_0$ for B_x and B_y states of TOP^{2+} calculated by TD-PBE1PBE. The z components for the partial derivatives of transition dipole moments are zero for all the in-plane modes. It was found from Table V that, as a whole, the B_{1g} modes have larger the partial derivatives than the B_{2g} modes.

By using the data in Tables I, IV and V, the B-band exited RR spectrum of TOP^{2+} can be calculated with Eqs.(1), (2), (6), and (7). Figure 2 displays the calculated RR spectra, in which the frequencies have been scaled by 0.959, 0.975, 0.956, and 0.972, respectively, for PBE1PBE, B3LYP, Cam-B3LYP, and B3LYP-D3. A 50:50 mixed Gauss-Lorentz line-shape was used in spectral plotted in Fig.2, with the band-width 12 cm^{-1}. It can be seen that the four XC-functionals produce similar RR spectra; and the relative RR intensities by TDDFT calculations are well consistent with the experiments. As shown in Fig.2 and Table III, the B-band excited RR spectra of TOP^{2+} are dominated by the totally symmetric A_{1g} modes, manifesting that the Franck-Condon mechanism (A-term mechanism) is prevailing for Raman enhancement. This is expectable since the excitation line is in near resonance with the transition from the ground state to the B-state which has a quite lager transition dipole moment (as shown in Table I). The ν_2, ν_6, ν_7, and ν_8 modes were calculated to be the strongest, in consistence with their large Δ values. These modes are assigned to the $C_\beta C_\beta$ stretching, furan breathing, furan in-plane symmetric deformation, and furan translational vibrations. From Fig.2, it can be seen that the relative intensities of the A_{1g} modes are in the order $\nu_6 > \nu_2 \approx \nu_8 > \nu_7 > \nu_4 > \nu_9 >> \nu_3$, which is fully consistent with the experiment. The RR enhancement pattern of the A_{1g} modes reflects the geometry change

DOI:10.1063/1674-0068/28/cjcp1504067

TABLE V TD-PBE1PBE/6-31G(d) calculated partial derivatives of transition dipole moments (in a.u.) with respect to the kth normal coordinates (in Å/Dalton$^{1/2}$) for the B_x and B_y states of TOP^{2+}. $\partial(\mu_{B_y})_x/\partial Q_k$=0, $\partial(\mu_{B_x)_y}/\partial Q_k$=0.

		Frequency[a]	$\frac{\partial(\mu_{B_y})_y}{\partial Q_k}$	$\frac{\partial(\mu_{B_x})_x}{\partial Q_k}$
A_{1g}	ν_2	1539	−0.02	0.01
	ν_3	1423	−0.04	0.03
	ν_4	1373	0.02	−0.03
	ν_9	1060	−0.03	0.02
	ν_6	928	0.04	−0.05
	ν_7	693	−0.02	0.01
	ν_8	292	0.05	−0.05
B_{1g}	ν_{10}	1649	0.07	0.04
	ν_{11}	1480	0.42	0.39
	ν_{12}	1378	0.18	0.18
	ν_{13}	1197	−0.01	−0.02
	ν_{17}	1059	0.15	0.14
	ν_{15}	965	0.10	0.09
	ν_{16}	720	0.09	0.08
	ν_{18}	135	0.04	0.04
B_{2g}	ν_{28}	1493	0.13	0.12
	ν_{29}	1310	−0.07	−0.08
	ν_{34}	1187	0.14	0.13
	ν_{30}	990	0.12	0.12
	ν_{32}	792	−0.01	−0.02
	ν_{33}	416	−0.02	−0.03
	ν_{35}	101	0.06	0.05

[a] PBE1PBE/6-31G(d) calculated frequencies (in cm^{-1}), scaling factor of 0.959.

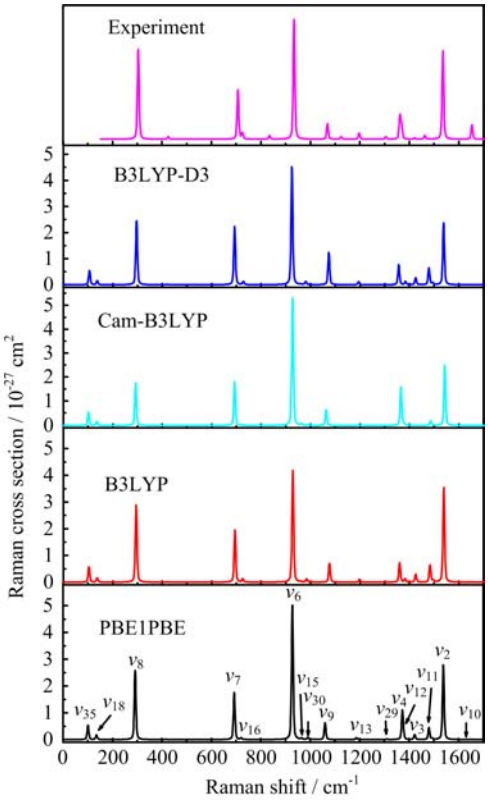

FIG. 2 The simulated B-band excited RR spectra of TOP^{2+} by TDDFT calculations. The incident lines were set at 3.5223 eV (PBE1PBE), 3.4510 eV (B3LYP), 3.5795 eV (Cam-B3LYP), and 3.4539 eV (B3LYP-D3), respectively. Experimental spectrum is adapted from the polarized RR spectrum in Ref.[11].

of the B state respect to ground state. The significant intensities of ν_2, ν_6, ν_7, and ν_8 modes come from the large Δ values, indicating a considerable deformation of the B state along these modes.

The non-totally symmetric modes can be enhanced through the Herzberg-Teller mechanism (B term). Figure 3 compares the A term, B term, and A/B terms contributions to the RR intensities of TOP^{2+}. The B_{1g} and B_{2g} modes, such as ν_{11}, ν_{12}, ν_{13}, ν_{17}, ν_{16}, ν_{18}, and ν_{35}, were calculated to be resonantly enhanced, but their intensities are one or two order weaker in comparison with the totally symmetric A_{1g} modes. This is in good accordance with the experiment. However, it is noteworthy that the calculated intensity of the ν_{10} mode ($C_\beta C_\beta$ stretch, B_{1g} symmetry) is considerably weaker as compared with the experiment. In the experiment, the ν_{10} mode was observed as the strongest depolarized band in the 406.7 nm excited RR spectrum [11]. Among the non-totally symmetric modes, the ν_{11} mode (asymmetric $C_\alpha C_m$ stretch, B_{1g} symmetry) was calculated to be resonance enhanced in a magnitude comparable to the totally symmetric ν_9 mode, which is obviously overestimated since the corresponding RR band was observed very weak in the experiment [11].

IV. DISCUSSION

The present calculation model for RR intensities assumes that (i) there is no Duschinsky rotation, *i.e.* normal mode compositions at excited state are the same as those at the ground state, and (ii) the force constants of excited and ground states are the same, *i.e.* the potential surface of excited state is shifted but not distorted in comparison with that of the ground state. However, the B state (2^1E_u) is doublet degenerate, and it may encounter the Jahn-Teller instability. The excited state Jahn-Teller effect in the Q-band has been reported for the normal metalloporphyrins and was recognized to be responsible for the dramatic enhancement of the B_{1g} and B_{2g} modes in Q-band excited RR spectra. When Jahn-Teller effect (either a static or dynamic one) occurs, both the normal mode compositions and the force constants of the excited state can significantly differ from those of the ground state. In this case, the

DOI:10.1063/1674-0068/28/cjcp1504067

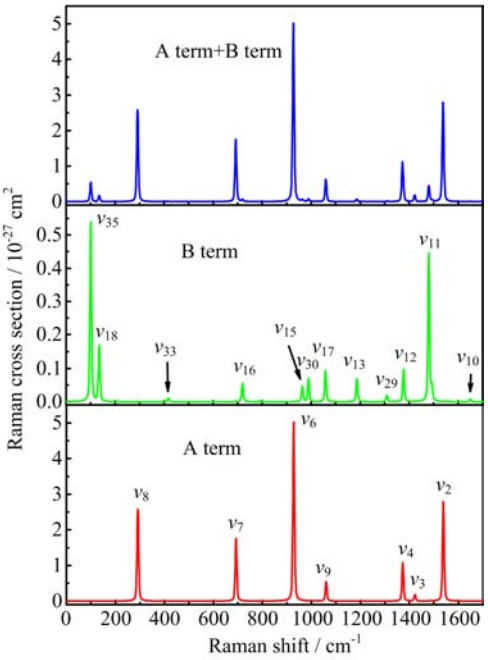

FIG. 3 TD-PBE1PBE/6-31G(d) calculated A term, B term, and A and B terms contributions for the B-band excited resonance Raman of TOP^{2+}, with the incident line at 3.5223 eV.

above mentioned approximations may not strictly hold. For TOP^{2+}, the discrepancy between the calculated and experimental RR intensities for the ν_{10} and ν_{11} modes may be attributed to the Jahn-Teller effect (presumably a dynamic one) of the B state (2^1E_u), which causes the ν_{10} and ν_{11} modes of the ground state to mix and reconstruct in the excited state.

In the present study, we did not consider the influence of the Q state (S_1 state). There are several reasons. Firstly, the energy separation between the Q state and the B state is quite large (1.01 eV by experiment and ∼1.44 eV by TD-PBE1PBE calculation) and the laser line used in the RR experiment is close to the B band (red-shift by only 0.33 eV). Secondly, the transition dipole moment of the Q band is much smaller compared with the B band by one-order of magnitude (from experiments) or more (from TDDFT). Thus the B-band resonance is expected to be dominating in the Raman process. The third, up to now, there are no experimental evidence of the inter-states (between the B and Q states) vibronic coupling for TOP^{2+}. This is different from the case of conventional metalloporphyrins for which the inter B and Q states vibronic coupling leads to the appearance of the A_{2g} bands (with abnormal depolarization ratios) in RR spectra and the 0-1 sub-band (Q_{01} band) in the UV-visible spectrum. In view of their close similarity in the geometric and electronic structures, this difference in the inter-states vibronic coupling between TOP^{2+} and metalloporphyrins is quite unusual and deserves to be studied in future.

V. CONCLUSION

In summary, DFT and TDDFT calculations have been used to study the resonance Raman spectra of TOP^{2+} with B-band excitation. Both Raman A and A terms are included in computation model, and it was found that the Raman A term is roughly one order of magnitude larger than Raman B term for the B band excitation. For this specific system of TOP^{2+}, the calculated RR spectra using PBE1PBE, B3LYP, Cam-B3LYP, and B3LYP-D3 XC-functionals are consistent with each other and agree well with the experiment. The strong intensities of the totally symmetric ν_2, ν_6, ν_7, and ν_8 modes indicating a considerable deformation of the B-state of TOP^{2+} along these mode. The RR intensity of the ν_{10} mode predicted by TDDFT calculations is unexpectedly small while the intensity of ν_{11} mode was calculated too large, which is attributed to the possible Jahn-Teller effect for the B state (*i.e.*, the 2^1E_u state) of TOP^{2+}.

VI. ACKNOWLEDGMENTS

This work was supported by the National Education Department of China (No.200803580022), the Science and Technology Bureau of Suzhou (No.ZXG2013004), and the Supercomputation Center of USTC.

[1] E. Vogel, W. Haas, B. Knipp, J. Lex, and H. Schmickler, Angew. Chem. Int. Ed. Engl. **27**, 406 (1988).
[2] E. Vogel, Pure Appl. Chem. **65**, 143 (1993).
[3] E. Vogel, J. Dörr, A. Herrmann, J. Lex, H. Schmickler, P. Walgenbach, J. P. Gisselbrecht, and M. Gross, Angew. Chem. Int. Ed. Engl. **32**, 1597 (1993).
[4] G. Miirkl, T. Knott, P. Kreitmeier, T. Burgemeister and F. Kastner, Tetrahedron **52**, 11763 (1996).
[5] I. Jelovica, L. Moroni, C. Gellini, P. R. Salvi, and N. Orlić, J. Phys. Chem. A **109**, 9935 (2005).
[6] A. Marcelli, P. Foggi, L. Moroni, C. Gellini, P. R. Salvi, and I. J. Badovinac, J. Phys. Chem. A **111**, 2276 (2007).
[7] R. Bachmann, F. Gerson, G. Gescheidt, and E. Vogel, J. Am. Chem. Soc. **114**, 10855 (1992).
[8] K. Malsch, M. Roeb, V. Karuth, and G. Hohlneicher, Chem. Phys. **227**, 331 (1998).
[9] J. Wan, Y. Ren, J. Wu, and X. Xu, J. Phys. Chem. A **108**, 9453 (2004).
[10] M. Xiang, G. H. Yao, T. T. Lu, T. J. He, and D. M. Chen, J. Mol. Struct. Theochem. **868**, 6 (2008).
[11] D. M. Chen, *PhD Dissertation*, Hong Kong: The Hong Kong University of Science and Technology, 319 (1997).
[12] X. Y. Li, R. S. Czernuszewicz, J. R. Kincaid, Y. O. Su, and T. G. Spiro, J. Phys. Chem. **94**, 31 (1990).
[13] X. Y. Li, R. S. Czernuszewicz, J. R. Kincaid, P. Stein, and T. G. Spiro, J. Phys. Chem. **94**, 47 (1990).
[14] X. Y. Li, R. S. Czernuszewicz, J. R. Kincaid, and T. G. Spiro, J. Am. Chem. Soc. **111**, 7012 (1989).

DOI:10.1063/1674-0068/28/cjcp1504067

[15] T. S. Rush, P. M. Kozlowski, C. A. Piffat, R. Kumble, M. Z. Zgierski, and T.G. Spiro, J. Phys. Chem. B **104**, 5020 (2000).
[16] D. M. Chen, T. J. He, D. F. Cong, Y. H. Zhang, and F. C. Liu, J. Phys. Chem. A **105**, 3981 (2001).
[17] H. L. Gao, F. Chen, C. L. Wang, G. B. Wang, and D. M. Chen, Chin. J. Chem. Phys. **26**, 398 (2013).
[18] T. T. Lu, T. J. He, F. C. Liu, and D. M. Chen, Chin. J. Chem. Phys. **23**, 573 (2010).
[19] Z. Y. Li, T. T. Lu, T. J. He, F. C. Liu, and D. M. Chen, Chin. J. Chem. Phys. **22**, 346 (2009).
[20] (a) J. Tang, and A. C. Albrecht, *in Raman Spectroscopy*, H. A. Szymanski, Ed., New York: Plenum Press, Vol.2, 33 (1970).
(b) P. M. Champion and A. C. Albrecht, Annu. Rev. Phys. Chem. **353**, 33 (1982).
[21] (a) O. S. Mortensen and S. Hassing, Adv. Infrared Raman Spectrosc. **6**, 1 (1980).
(b) S. Hassing, J. Raman Spectro. **28**, 739 (1997).
[22] (a) A. Washel and P. Dauber, J. Chem. Phys. **66**, 5477 (1977).
(b) L. Chinsky, A. Laigle, W. L. Peticolas, and P. Y. Turpin, J. Chem. Phys. **76**, 1 (1982).
[23] L. Jensen and G. C. Schatz, J. Phys. Chem. A **110**, 5973 (2006).
[24] R. H. Zheng, W. M. Wei, L. L. Zhua, and Q. Shi, Spectrochimica Acta A **133**, 707 (2014).
[25] A. B. Myers, Chem. Rev. **96**, 911 (1996).
[26] A. M. Moran, C. Delbecque, and A. M. Kelly, J. Phys. Chem. A **105**, 10208 (2001).
[27] A. M. Kelly, J. Phys. Chem. A **112**, 11975 (2008).
[28] B. Mennucci, C. Cappelli, R. Cammi, and J. Tomasi, Theor. Chem. Acc. **117**, 1029 (2007)
[29] M. J. Frisch, G. W. Trucks, H. B. Schlegel, G. E. Scuseria, M. A. Robb, J. R. Cheeseman, G. Scalmani, V. Barone, B. Mennucci, G. A. Petersson, H. Nakatsuji, M. Caricato, X. Li, H. P. Hratchian, A. F. Izmaylov, J. Bloino, G. Zheng, J. L. Sonnenberg, M. Hada, M. Ehara, K. Toyota, R. Fukuda, J. Hasegawa, M. Ishida, T. Nakajima, Y. Honda, O. Kitao, H. Nakai, T. Vreven, J. A. Jr. Montgomery, J. E. Peralta, F. Ogliaro, M. Bearpark, J. J. Heyd, E. Brothers, K. N. Kudin, V. N. Staroverov, T. Keith, R. Kobayashi, J. Normand, K. Raghavachari, A. Rendell, J. C. Burant, S. S. Iyengar, J. Tomasi, M. Cossi, N. Rega, J. M. Millam, M. Klene, J. E. Knox, J. B. Cross, V. Bakken, C. Adamo, J. Jaramillo, R. Gomperts, R. E. Stratmann, O. Yazyev, A. J. Austin, R. Cammi, C. Pomelli, J. W. Ochterski, R. L. Martin, K. Morokuma, V. G. Zakrzewski, G. A. Voth, P. Salvador, J. J. Dannenberg, S. Dapprich, A. D. Daniels, Ö. Farkas, J. B. Foresman, J. V. Ortiz, J. Cioslowski, and D. J. Fox, *Gaussian 09, Revision D.01*, Wallingford CT: Gaussian, Inc., (2013).
[30] A. D. Becke, J. Chem. Phys. **98**, 5648 (1993).
[31] C. Lee, W. Yang, and R. G. Parr, Phys. Rev. B **37**, 785 (1988).
[32] (a) J. P. Perdew, K. Burke, and M. Ernzerhof, Phys. Rev. Lett. **77**, 3865 (1996).
(b) J. P. Perdew, K. Burke, and M. Ernzerhof, Phys. Rev. Lett. **78**, 1396 (1997).
[33] T. Yanai, D. Tew, and N. Handy, Chem. Phys. Lett. **393**, 51 (2004).
[34] J. Moellmann and S. Grimme, PCCP **12**, 8500 (2010).
[35] Z. Y. Li, H. L. Wang, T. T. Lu, T. J. He, F. C. Liu, and D. M. Chen, Spectrochim. Acta A **67**, 1382 (2007).

DOI:10.1063/1674-0068/28/cjcp1504067